



# Impaired Interleukin-27–Mediated Control of CD4+ T Cell Function Impact on Ectopic Lymphoid Structure Formation in Patients With Sjögren’s Syndrome

Davide Lucchesi,<sup>1</sup>  Rachel Coleby,<sup>1</sup>  Elena Pontarini,<sup>1</sup>  Edoardo Prediletto,<sup>1</sup>  Felice Rivellesse,<sup>1</sup>   
David G. Hill,<sup>2</sup> Alicia Derrac Soria,<sup>3</sup> Simon A. Jones,<sup>3</sup>  Ian R. Humphreys,<sup>3</sup>  Nurhan Sutcliffe,<sup>4</sup>  
Anwar R. Tappuni,<sup>5</sup>  Costantino Pitzalis,<sup>1</sup>  Gareth W. Jones,<sup>6</sup>  and Michele Bombardieri<sup>1</sup> 

**Objective.** Ectopic lymphoid structures (ELS) develop at sites of infection, autoimmunity, and cancer. In patients with Sjögren’s syndrome (SS), ELS support autoreactive B cell activation and lymphomagenesis. Interleukin-27 (IL-27) is a key regulator of adaptive immunity and limits Th17 cell–driven pathology. We undertook this study to elucidate the role of IL-27 in ELS formation and function in autoimmunity using a murine model of sialadenitis and in patients with SS.

**Methods.** ELS formation was induced in wild-type and *Il27ra*<sup>−/−</sup> mice via salivary gland (SG) cannulation of a replication-deficient adenovirus in the presence or absence of IL-17A neutralization. In SG biopsy samples, IL-27–producing cells were identified by multicolor immunofluorescence microscopy. Lesional and circulating IL-27 levels were determined by gene expression and enzyme-linked immunosorbent assay. The in vitro effect of IL-27 on T cells was assessed using fluorescence-activated cell sorting and cytokine release.

**Results.** In experimental sialadenitis, *Il27ra*<sup>−/−</sup> mice had larger and more hyperactive ELS (focus score;  $P < 0.001$ ), increased autoimmunity, and an expanded Th17 response ( $P < 0.001$ ), compared to wild-type mice. IL-17 blockade in *Il27ra*<sup>−/−</sup> mice suppressed the aberrant ELS response (B and T cell reduction against control;  $P < 0.01$ ). SS patients displayed increased circulating IL-27 levels ( $P < 0.01$ ), and in SG biopsy samples, IL-27 was expressed by DC-LAMP+ dendritic cells in association with CD3+ T cells. Remarkably, in SS T cells (but not in T cells from patients with rheumatoid arthritis or healthy controls), IL-27–mediated suppression of IL-17 secretion was severely impaired and associated with an aberrant interferon- $\gamma$  release upon IL-27 stimulation.

**Conclusion.** Our data indicate that the physiologic ability of IL-27 to limit the magnitude and function of ELS through control of Th17 cell expansion is severely impaired in SS patients, highlighting a defective immunoregulatory checkpoint in this condition.

## INTRODUCTION

Infection, autoimmunity, and cancer can induce a state of inflammation in nonlymphoid tissues that can lead to the antigen-driven formation of lymphoid structures at these ectopic sites (1).

This process, ectopic lymphoneogenesis, culminates with the formation of ectopic lymphoid structures (ELS). ELS are characterized by B cell and T cell infiltrates that are often organized into germinal center (GC)–like structures with segregated B cell and T cell areas, follicular dendritic cell (FDC) networks, and other

Supported by Versus Arthritis (reference 21268 to Dr. Bombardieri) and the Medical Research Council (grant MR/N003063/1 to Dr. Bombardieri). Dr. Pontarini is a Foundation Fellow whose work is supported by Versus Arthritis (reference 21753). Dr. Hill’s work is supported by a Medical Research Council PhD studentship and by the Life Sciences Research Network Wales. Dr. Jones is a Career Development Fellow whose work is supported by Versus Arthritis (reference 20305).

<sup>1</sup>Davide Lucchesi, PhD, Rachel Coleby, MSc, Elena Pontarini, PhD, Edoardo Prediletto, MSc, Felice Rivellesse, MD, PhD, Costantino Pitzalis, FRCP, MD, PhD, Michele Bombardieri, MD, PhD: Queen Mary University of London, London, UK; <sup>2</sup>David G. Hill, PhD: Cardiff University, Cardiff, UK, and University of Bristol, Bristol, UK; <sup>3</sup>Alicia Derrac Soria, BSc, Simon A. Jones, PhD, Ian R. Humphreys, PhD: Cardiff University, Cardiff, UK; <sup>4</sup>Nurhan Sutcliffe, FRCP, MD: Barts Health NHS Trust, London, UK; <sup>5</sup>Anwar R. Tappuni, LDSRCS, PhD:

Queen Mary University of London, London, UK; <sup>6</sup>Gareth W. Jones, PhD: University of Bristol, Bristol, UK.

Drs. Lucchesi and Pontarini and Ms Coleby contributed equally to this work.

No potential conflicts of interest relevant to this article were reported.

Address correspondence to Michele Bombardieri, MD, PhD, Centre for Experimental Medicine & Rheumatology, William Harvey Research Institute, John Vane Science Centre, Queen Mary University of London, Charterhouse Square, London EC1M 6BQ, UK (email: m.bombardieri@qmul.ac.uk); or to Gareth W. Jones, PhD, School of Cellular and Molecular Medicine, Biomedical Sciences Building, University of Bristol, Bristol BS8 1TD, UK (email: g.jones@bristol.ac.uk).

Submitted for publication October 7, 2019; accepted in revised form April 14, 2020.

markers of GC activity (1,2). Whereas in cancer and infection ELS can often have a protective role, in autoimmunity, ectopic lymphoneogenesis is associated with more aggressive inflammation and worse prognosis (1,3) due to the ability of ELS to provide a local niche for the survival of autoreactive T cells, B cells, and plasma cells. In Sjögren's syndrome (SS), an autoimmune exocrinopathy with prevalent salivary gland (SG) involvement (4,5), ELS form in 20–40% of patients (6) and are associated with higher systemic disease severity (7) and the development of parotid B cell mucosa-associated lymphoid tissue type lymphomas, albeit with some controversy (8–12).

Interleukin-27 (IL-27) is a heterodimeric cytokine composed of IL-27p28 and Epstein-Barr virus-induced gene 3 (EBI-3) subunits, the latter being shared with IL-35. IL-27 signals through a receptor complex comprising a unique IL-27 receptor  $\alpha$  (IL-27R $\alpha$ ) chain, and the common IL-6 family signaling receptor, gp130 (13,14). In infection, IL-27 regulates both innate and adaptive immunity (14–17). IL-27 was initially described as a proinflammatory cytokine that promotes Th1 cell differentiation and cytotoxic CD8+ T cell responses through regulation of T-bet (18,19). Subsequently, IL-27 was shown to modulate T cell hyperactivation (16,20), regulation of IL-2 (21,22), IL-10 (23), and IL-22 (24) production in CD4+ T cells (25), induction of B cell class-switching (26), and regulation of Th17 and Treg cell differentiation (27–31).

To determine the role of IL-27 in modulating the magnitude and functionality of ELS, we used a murine model of SG inflammation featuring ELS formation and breach of self-tolerance (32), focusing on the ability of IL-27 to regulate the expansion of IL-17A-producing T cells. To extend the observations from our model to autoimmunity, we also characterized the systemic and SG presence of IL-27 in SS patients and measured the ability of SS-derived peripheral blood CD4+ T cells to respond to IL-27 stimulation *in vitro*.

## MATERIALS AND METHODS

**Human samples.** Experiments using samples from human subjects were performed on blood and SG tissue collected from 54 consecutive SS patients and 45 nonspecific chronic sialadenitis patients visiting a specialist rheumatology/oral medicine clinic at Barts Health NHS Trust (see Supplementary Table 1, on the *Arthritis & Rheumatology* website at <http://onlinelibrary.wiley.com/doi/10.1002/art.41289/abstract>). All procedures were approved by the local ethics committee (LREC 05/Q0702/1 and LREC 17/WS/0172) and performed after obtaining informed written consent. For the histologic classification of SG tissue, 5- $\mu$ m paraffin-embedded sections were stained with hematoxylin and eosin (H&E) to determine the infiltrate focus score (number of cellular aggregates with >50 cells per 4 mm<sup>2</sup> of gland tissue). The level and quality of SG immune cell infiltration was characterized by immunohistochemistry, in order to assess the degree of T cell (CD3), B cell (CD20), and plasma cell (CD138) infiltration and the

presence of FDC networks (CD21) (Supplementary Figure 1A, <http://onlinelibrary.wiley.com/doi/10.1002/art.41289/abstract>).

Patients were classified as ELS+ if the SG biopsy sample showed  $\geq 1$  infiltrate with clear B cell/T cell segregation and positive CD21 staining (33). Demographic data for SS patients with characterized histology is provided in Supplementary Table 2 (<http://onlinelibrary.wiley.com/doi/10.1002/art.41289/abstract>). The effects of IL-27 stimulation were determined *in vitro* by treating peripheral blood mononuclear cells (PBMCs) from a subcohort of SS patients, rheumatoid arthritis (RA) patients, and age- and sex-matched healthy donors with increasing doses of recombinant IL-27. Demographic data for this subcohort is provided in Supplementary Table 1.

**Animals and treatment.** All procedures were performed with ethical approval (PPL 70/8259 and P7867DADD) from the Home Office and local animal welfare committees. *Il27ra*<sup>-/-</sup> mice have been described previously (34). Female *Il27ra*<sup>-/-</sup> mice and wild-type (WT) control mice on the C57BL/6 background were bred and maintained under pathogen-free conditions at Cardiff University, or acquired from Charles River and maintained in the Biomedical Service Unit at Queen Mary University of London. For adenovirus cannulation (32) of the SGs, mice were anesthetized by administration of ketamine (60 mg/kg) and xylazine (12 mg/kg) intraperitoneally. Analgesia was provided as 0.1 mg/kg buprenorphine hydrochloride via subcutaneous injection. The submandibular gland was cannulated through the excretory duct using heat-drawn glass gas chromatography tubing (0.1-mm internal diameter; Sigma-Aldrich). Approximately 20  $\mu$ l adenovirus solution, equivalent to  $\geq 10^{10}$  plaque-forming units of reporter-encoding adenovirus, was injected into the submandibular gland using an attached Hamilton syringe (Sigma-Aldrich). For IL-17A blockade, mouse anti-mouse IL-17A antibody (clone 17F3; BioXell) or matched isotype control (clone MOPC21; BioXell) was administered intraperitoneally at 500  $\mu$ g per mouse every 3 days, starting from the day before virus infection.

**Gene expression.** Total RNA was extracted from tissue using an RNeasy Mini kit (Qiagen) and from murine CD11b+ cells using an Arcturus PicoPure RNA kit (ThermoFisher). Complementary DNA (cDNA) was synthesized with a ThermoScript System (Invitrogen). For whole tissue analysis, samples were run in duplicate at 5 ng cDNA/well, detected using an ABI PRISM 7900HT instrument, and results were analyzed using an ABI PRISM Sequence Detection System, version 2.1. For isolated CD11b+ cells, cDNA samples were run at 5 ng cDNA/well using Applied Biosystems TaqMan probes on a Biomark HD instrument and analyzed with real-time polymerase chain reaction (PCR) analysis software (both from Fluidigm). Primers and probes for quantitative TaqMan real-time PCR were obtained from Applied Biosystems (Supplementary Table 3, <http://onlinelibrary.wiley.com/doi/10.1002/art.41289/abstract>). Relative quantification

was assessed by the comparative threshold cycle method using 18S (human samples and murine myeloid cells) or *Hprt* genes (murine tissue samples) as housekeeping genes. Relative quantitation was calibrated using a selected lymph node cDNA for murine samples, and a patient with sicca symptoms was selected for human experiments.

**Isolation of leukocytes from tissue and blood.** Murine SGs were digested in medium containing collagenase D (Roche) and DNase I (Sigma-Aldrich). CD11b<sup>+</sup> cells were obtained with a positive magnetic selection kit (EasySep). PBMCs were isolated from human blood by density gradient (Lymphoprep; StemCell Technologies). For pSTAT staining and cell surface IL-27R $\alpha$  detection, cells were used directly after isolation. IL-27 stimulation of human PBMCs is described in the Supplementary Methods (<http://onlinelibrary.wiley.com/doi/10.1002/art.41289/abstract>).

**Flow cytometry.** For cytokine detection, single-cell suspensions were first stimulated for 4 hours at 37°C in the presence of Leukocyte Activation Cocktail (BD Biosciences). Cells were then incubated with a live/dead exclusion dye (Aqua Zombie; BioLegend) followed by Fc receptor blocking solution (TruStain; BioLegend) and surface antibodies mix (Supplementary Table 4, <http://onlinelibrary.wiley.com/doi/10.1002/art.41289/abstract>). Cells were washed, fixed, and permeabilized (eBioscience FoxP3 fixation/permeabilization kit; ThermoFisher) and stained with intracellular antibodies mix (Supplementary Table 4). Cells were then washed and acquired. When an absolute count was required, Invitrogen CountBright counting beads (ThermoFisher) were used. For detection of pSTAT1 and pSTAT3, PBMCs were incubated in medium-containing surface antibodies (Supplementary Table 2, <http://onlinelibrary.wiley.com/doi/10.1002/art.41289/abstract>) in the presence or absence of 40 ng/ml human IL-27 for 15 minutes at 37°C. Cells were then fixed in paraformaldehyde, permeabilized in 90% methanol, and incubated with pSTAT1- and pSTAT3-specific antibodies. Events were acquired on an LSR Fortessa cytometer (BD Biosciences) within 24 hours, and analysis was performed using FlowJo X. For human experiments, events were gated on viable cells, while murine samples were gated for viable/CD45<sup>+</sup> cells. Where relevant, a dump channel was used to exclude nonrelevant populations (human panels V510/20, murine panels R780/60).

**Histology and immunofluorescence.** Detailed methods for slide preparation from frozen and paraffin-embedded tissue blocks are provided in the Supplementary Methods (<http://onlinelibrary.wiley.com/doi/10.1002/art.41289/abstract>). See Supplementary Table 4 for a list of fluorochrome-conjugated primary antibodies used for immunofluorescence staining.

Three-micrometer sections from human formalin-fixed paraffin-embedded tonsillectomies and minor SGs from SS patients underwent deparaffinization and target retrieval and

were stained with primary antibodies (Supplementary Table 4) and detected using fluorescent secondary antibodies. Nuclei were counterstained with DAPI, and slides were mounted with ProLong Gold medium. Digital image analysis was performed using Fiji and Qupath (35,36).

**Protein detection in sera and supernatants.** IL-27 levels in the undiluted sera of patients with SS and those with sicca symptoms were quantified by enzyme-linked immunosorbent assay (ELISA) (no. DY2526) according to the instructions of the manufacturer (R&D Systems). Interferon- $\gamma$  (IFN $\gamma$ ) in cell culture supernatants was quantified using a human IFN $\gamma$  ELISA kit (no. 430104; BioLegend). For this, supernatants were diluted 1:5,000 or 1:10,000, and biologic duplicates were pooled and quantified in technical duplicates. For the detection of IL-17A, IL-17F, IL-21, and IL-22 in undiluted cell culture supernatants, a customized multiplex liquid phase immunoassay (LegendPlex) was used according to the instructions of the manufacturer (BioLegend).

**Detection of antiadenovirus and antinuclear antibodies (ANAs) in serum.** Ninety-six half-well ELISA plates (Corning) were coated overnight at 4°C with either 5  $\mu$ g/ml adenovirus solution (anti-adenovirus ELISA) or 10  $\mu$ g/ml nuclear extract obtained from a HEp-2 cell line (ANA ELISA). For the ANA ELISA, the purity of the extract was assessed by Western blotting with antibodies against laminin  $\alpha$  and tubulin (Supplementary Methods and Supplementary Figure 2, <http://onlinelibrary.wiley.com/doi/10.1002/art.41289/abstract>). For the antiadenovirus antibody ELISA, a standard curve was created using serial dilutions of pooled sera from adenovirus-cannulated mice culled at 19 days post-cannulation. For the ANA ELISA, a standard curve was created using serial dilutions of pooled sera from MRL-*lpr/lpr* mice that spontaneously develop a wide range of autoantibodies. Murine sera were diluted to working concentration in 1% bovine serum albumin and 0.05% Tween 20 in phosphate buffered saline and plated in technical duplicates.

Class-specific antibodies were detected by adding biotinylated anti-mouse IgG1 or IgG2 detection antibodies followed by horseradish peroxidase-conjugated streptavidin (both from BioLegend). Antibodies were detected by incubation with tetramethylbenzidine substrate (BioLegend), and absorbance was read at 450 nm. Standard curves were calculated using a 4-parameter logistic regression, and the concentrations of unknown samples were calculated and expressed as arbitrary units.

**Statistical analysis.** Differences in quantitative variables between 2 groups were analyzed by Mann-Whitney 2-tailed U test. For multiple comparisons, Kruskal-Wallis test with Dunn's post hoc correction was used. In experiments with matched observations, Friedman's test with Dunn's correction was used. All statistical analyses were performed using GraphPad Prism, version 7.04. *P* values less than 0.05 were considered significant.

## RESULTS

**Stepwise IL-27 induction in murine SG-infiltrating immune cells following viral infection.** To investigate the control of SG inflammation by IL-27, we utilized a well-established model of inducible sialadenitis, characterized by an early activation of the resident stroma and innate immune cells, followed by accumulation of T cells and B cells, and the formation of ELS with functional GCs (32,37,38) (Supplementary Figure 3A, <http://onlinelibrary.wiley.com/doi/10.1002/art.41289/abstract>).

In whole-gland gene expression profiling, *Il27p28* messenger RNA (mRNA) was strongly induced by adenovirus infection, peaking as early as 5 days post-cannulation followed by a progressive decrease, but with a sustained expression throughout the course of the infection (Figure 1A). Consistent with previous evidence

describing antigen-presenting cells as a prominent source of IL-27 (39), *Il27p28* expression was strongly up-regulated in infiltrating CD11b+ myeloid cells at 5 days post-cannulation, but decreased to baseline thereafter (Figure 1B). Flow cytometry of digested SGs confirmed this observation (Figure 1C).

Interestingly, in uninfected SGs, expression of IL-27p28 was mostly confined to CD45- epithelial cell adhesion molecule-positive (EpcAM+) cells (Figure 1D), while CD45+ hematopoietic cells were the main source in adenovirus-infected glands (Figure 1E). Specifically, by 12 days post-cannulation, CD4+ and CD8+ T cells, natural killer cells, and B cells were the main IL-27-producing CD45+ subsets in the SGs, both in terms of absolute numbers and as a percentage of IL-27-producing leukocytes (Figure 1F and Supplementary Figure 3D, <http://onlinelibrary.wiley.com/doi/10.1002/art.41289/abstract>). These subsets

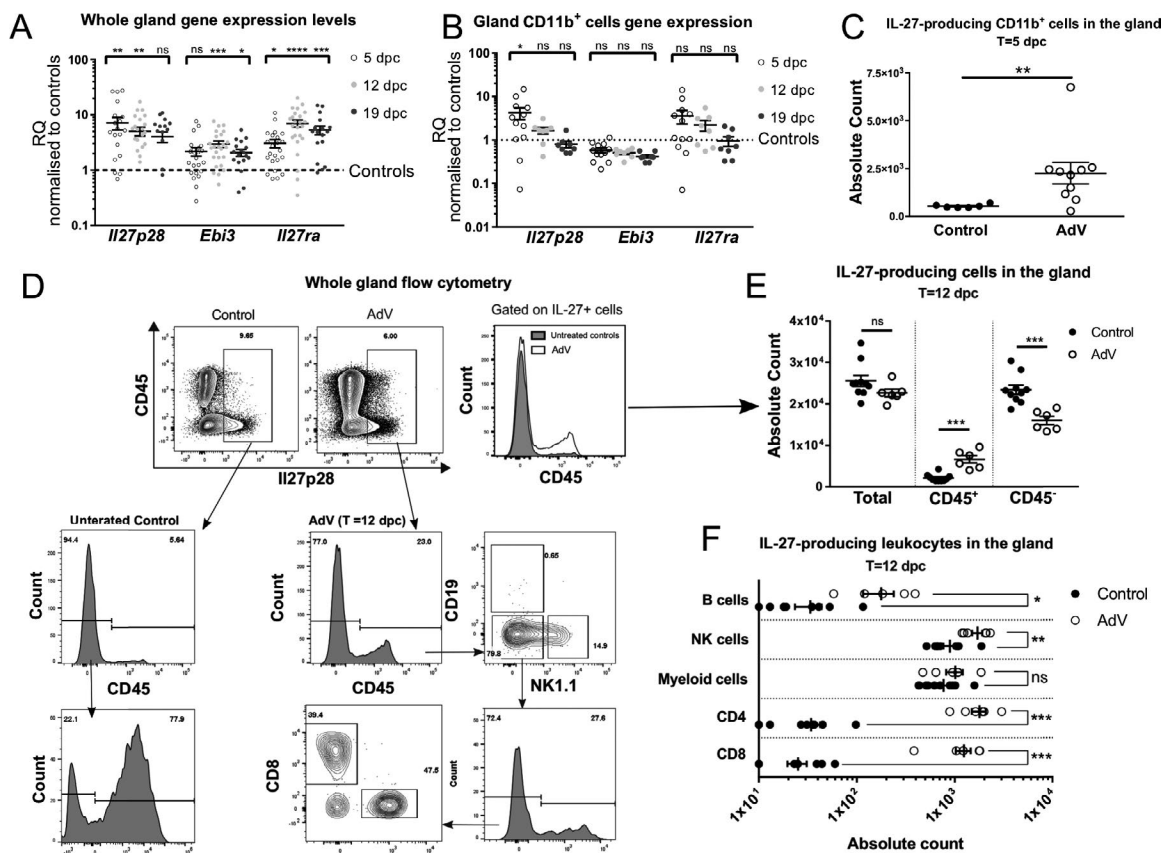


**Figure 1.** Interleukin-27 (IL-27) is produced in the murine salivary gland (SG) at the steady state and upon viral challenge. **A**, Expression of IL-27 subunits and the IL-27 receptor (*Il27p28*, *Ebi3*, and *Il27ra*, respectively), determined by real-time quantitative polymerase chain reaction in whole SG tissue at the steady state ( $n = 14$ ) and at 5 days ( $n = 23$ ), 12 days ( $n = 25$ ), and 19 days ( $n = 19$ ) post-cannulation (dpc). **B**, *Il27p28*, *Ebi3*, and *Il27ra* expression in sorted CD11b<sup>+</sup> myeloid cells at 5 days ( $n = 12$ ), 12 days ( $n = 8$ ), and 19 days ( $n = 8$ ) post-cannulation. **C**, Absolute cell counts of IL-27p28-producing CD11b<sup>+</sup> cells based on flow cytometry of enzymatically digested infected SGs ( $n = 10$ ) and uninfected SGs ( $n = 6$ ) at 5 days post-cannulation. **D**, Representative plots showing gating strategy for IL-27p28-producing viable single cells in the CD45<sup>-</sup> and CD45<sup>+</sup> populations (left) and overlay histograms of the IL-27p28-producing cells in untreated and adenovirus (AdV)-challenged mice (right). **E**, Absolute cell counts of IL-27p28-producing cells based on flow cytometry of enzymatically digested infected SGs ( $n = 6$ ) and uninfected SGs ( $n = 10$ ) at 12 days post-cannulation. **F**, Absolute count of the main IL-27p28-producing CD45<sup>+</sup> subpopulations present in inflamed SGs. Symbols represent individual mice; bars show the mean  $\pm$  SEM. \* =  $P < 0.05$ ; \*\* =  $P < 0.01$ ; \*\*\* =  $P < 0.001$ ; \*\*\*\* =  $P < 0.0001$  versus controls, by Kruskal-Wallis multiple comparison test in **A** and **B** and by Mann-Whitney U test in **C**, **E**, and **F**. RQ = relative quantification; NS = not significant; Epcam = epithelial cell adhesion molecule; NK = natural killer.

also showed an increase in the mean fluorescence intensity of IL-27 staining in fluorescence-activated cell sorting (Supplementary Figure 3C), suggesting an increase not only in the number of IL-27-producing cells but also an overall increase in the levels of IL-27 produced. A pie chart representing the individual contributions of the various immune cells subsets is presented in Supplementary Figure 3D. A decrease in the number of IL-27+ epithelial cells appears related to the abundant cell death among EpCAM+ SG epithelial cells upon infection (Supplementary Figure 3E). Overall, these data demonstrate that upon viral infection in the SGs, different cell types become able to produce IL-27 at diverse stages of the inflammatory and lymphoneogenic process.

**Up-regulation of IL-27 in SGs of SS patients with ELS, mainly produced by DC-LAMP+ dendritic cells in T cell-rich areas.** In our previous work, reduced levels of IL-27 mRNA in the inflamed joints of RA patients were associated

with a higher incidence of ELS, suggesting that an intrinsic defect in IL-27 may favor ELS formation in the inflamed joints (40). However, when we analyzed IL-27-related gene transcripts in the SGs of SS patients, we observed a significantly higher expression of *IL27p28*, *EBI3*, and *IL27Ra* mRNA, compared to patients with nonspecific chronic sialadenitis (sicca) who develop exocrine dysfunction without the autoimmune component typical of SS (Figure 2A). Unexpectedly, when we separated SS patients into ELS+ and ELS- groups based on SG immunohistology (Supplementary Figure 1A, <http://onlinelibrary.wiley.com/doi/10.1002/art.41289/abstract>), ELS+ patients displayed higher expression levels of *IL27*, *EBI3*, and *IL27RA*, compared to ELS- patients (Figure 2B), while there was no difference between ELS- SS patients and ELS- sicca patients. This was also confirmed by the positive correlation of the percentage of infiltrating B cells, T cells, and plasma cells with gene expression for the IL-27 signaling cassette (Figure 2C). Conversely, although we observed higher serum levels of

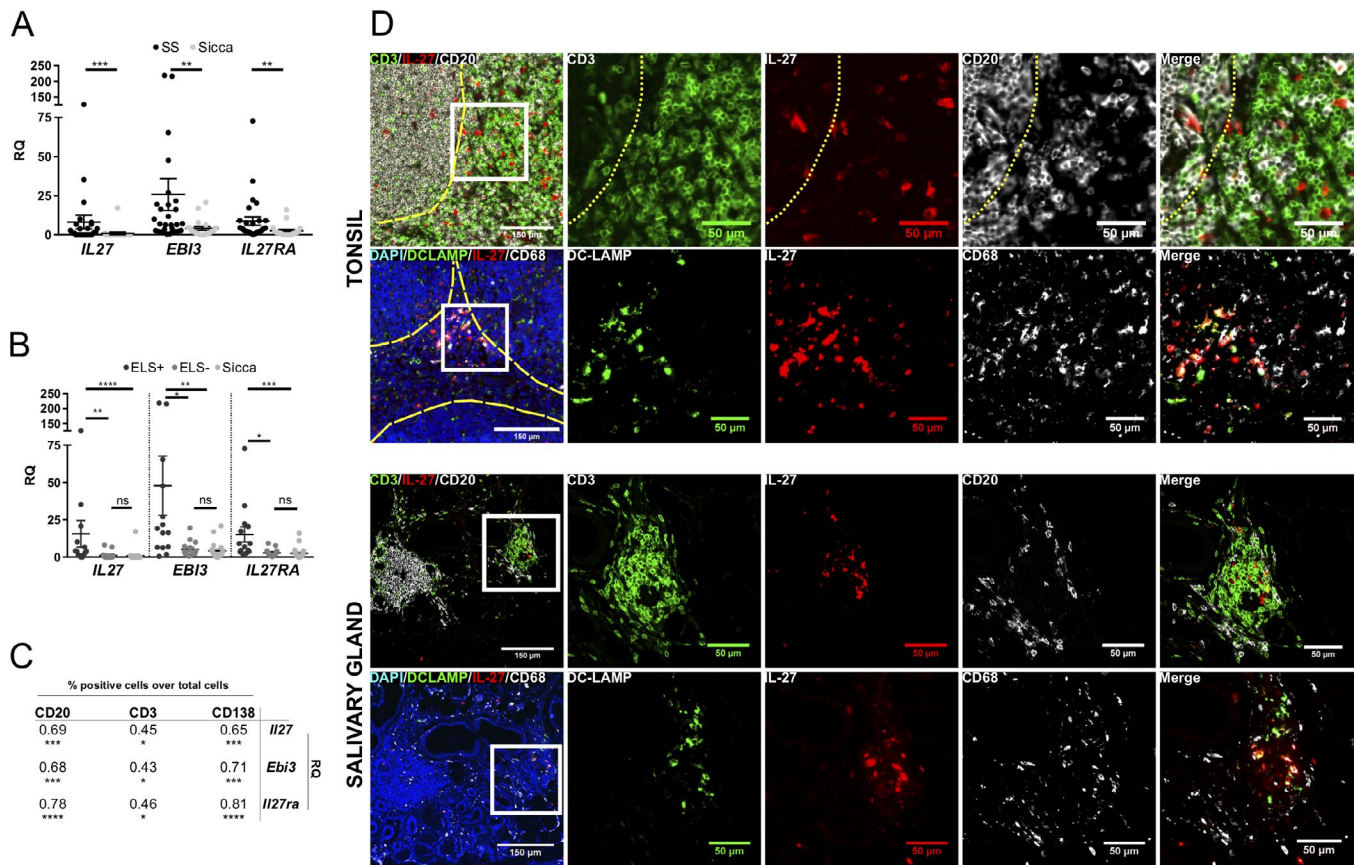


**Figure 2.** DC-LAMP+ dendritic cells are the main producer of IL-27 in human tonsil and SG ectopic lymphoid structures (ELS). **A** and **B**, Real-time quantitative polymerase chain reaction gene expression for *IL27*, *EBI3*, and *IL27RA* in patients with Sjögren's syndrome (SS) ( $n = 29$ ) and patients with nonspecific chronic sialadenitis (sicca) ( $n = 20$ ) (**A**) and in ELS+ SS patients ( $n = 14$ ) and ELS- SS patients ( $n = 15$ ) (**B**) on RNA extracted from SG biopsy samples. **C**, Spearman's correlation table showing rho values between *IL27*, *EBI3*, and *IL27RA* gene expression and the percentage of cells positive for CD20, CD3, and CD138 over total cells detected in minor SG histologic sections from SS and sicca patients. **D**, Representative immunofluorescence staining of paraffin-embedded sections from human tonsils and SGs from ELS+ SS patients. Top row shows staining for CD3+ T cells (green), IL-27p28 (red), and CD20+ B cells (white); bottom row shows staining for DC-LAMP+ dendritic cells (green), IL-27p28 (red), and CD68+ macrophages (white). Nuclei counterstained with DAPI (blue). Split channel and merge panels show higher-magnification views of the boxed areas. In **A** and **B**, symbols represent individual patients; bars show the mean  $\pm$  SEM. \* =  $P < 0.05$ ; \*\* =  $P < 0.01$ ; \*\*\* =  $P < 0.001$ ; \*\*\*\* =  $P < 0.0001$ , by Mann-Whitney U test in **A** and by Kruskal-Wallis test in **B**. See Figure 1 for other definitions.

IL-27 in SS patients compared to those with sicca, there was no difference when comparing the ELS+ and ELS- subsets (Supplementary Figures 1B and C).

Similar to findings in mouse SGs following viral infection, multicolor immunofluorescence identified many IL-27p28-producing cells with a dendritic morphology localized in the T cell-rich areas surrounding B cell follicles and in close contact with CD3+ T cells in both the inflamed tonsils and ELS+ SGs of SS patients (Figure 2D). Most of the IL-27p28-producing cells in ELS+ SGs and in tonsils were in fact DC-LAMP+ dendritic cells (Figure 2D) and not CD68+ macrophages, CD3+ T cells, or CD20+ B cells, confirming that in both mouse and human inflamed SG tissues, IL-27 is mainly produced by cells of myeloid lineage. Importantly, we

were able to identify by flow cytometry IL-27R $\alpha$ -positive mononuclear cells in the minor SG infiltrate in SS patients. Interestingly, among the cells positive for IL-27R $\alpha$  in the gland, the majority were CD4+ T cells (Supplementary Figure 1F, <http://onlinelibrary.wiley.com/doi/10.1002/art.41289/abstract>), which confirms that the inflammatory microenvironment of SS SGs harbors both IL-27-producing and IL-27-responsive cells.

**Impaired IL-27 signaling in *Il27ra*<sup>-/-</sup> mice promotes aberrant ELS formation and activity during viral-induced sialadenitis.** We next investigated the incidence, quantitative spatial composition, and function of ELS forming in SGs in *Il27ra*<sup>-/-</sup> mice versus WT mice following adenovirus infection. ELS

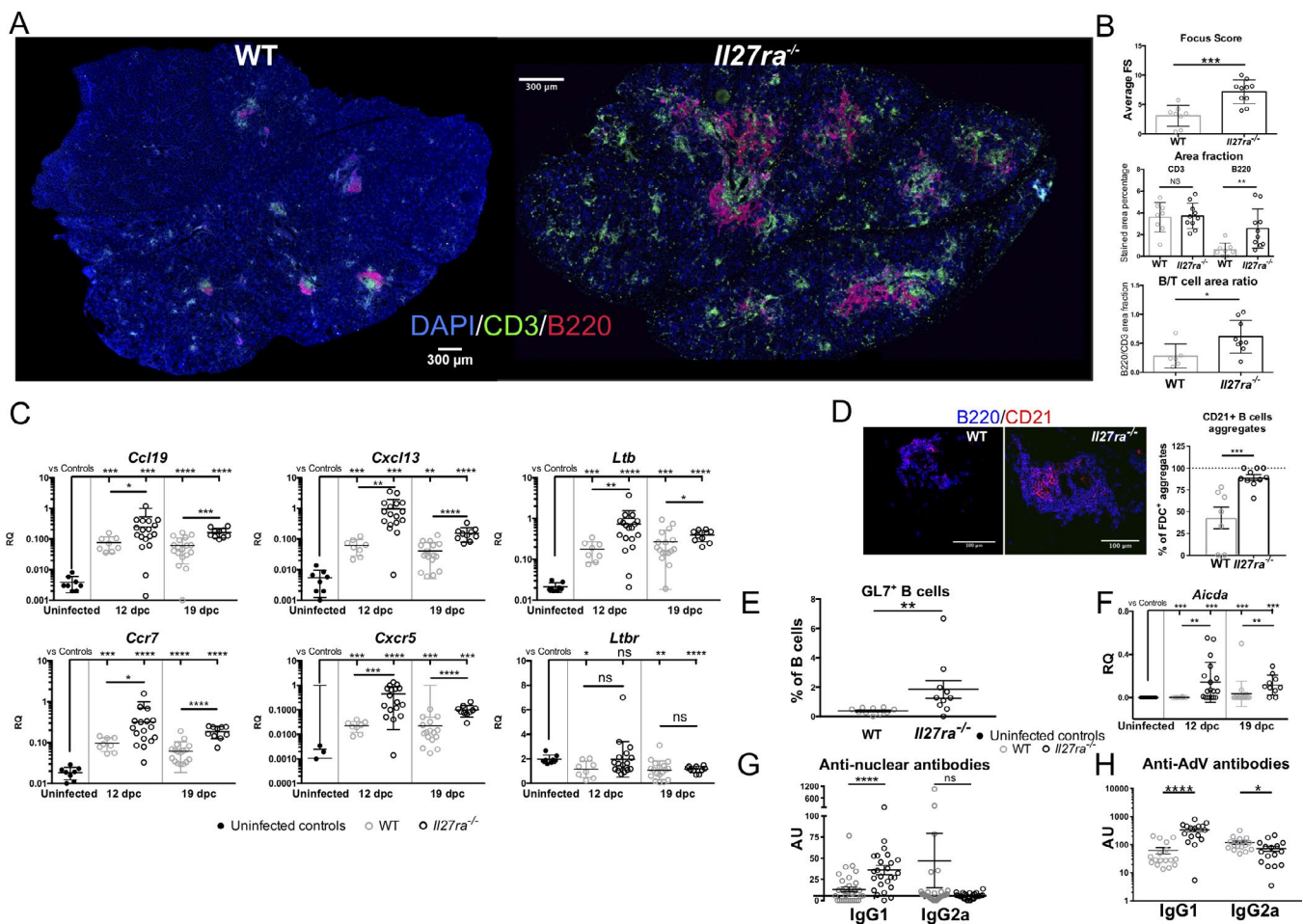


**Figure 3.** Inflamed SGs in *Il27ra*<sup>-/-</sup> mice show increased ectopic lymphoid structure (ELS) formation and germinal cell markers. **A**, Representative immunofluorescence for B220+ B cells and CD3+ T cells in SGs from adenovirus-treated wild-type (WT) mice (n = 8 glands) and *Il27ra*<sup>-/-</sup> mice (n = 10 glands) at 19 days post-cannulation. **B**, Average focus score (FS) of 3 cutting levels (60  $\mu$ m apart) per gland (WT n = 8, *Il27ra*<sup>-/-</sup> n = 10), area fraction of SG staining positive for B cells and T cells (WT n = 8, *Il27ra*<sup>-/-</sup> n = 10), and the ratio between B cell and T cell areas (WT n = 6, *Il27ra*<sup>-/-</sup> n = 9). **C**, Gene expression analysis of SGs from uninfected controls (n = 8) and adenovirus-infected WT mice and *Il27ra*<sup>-/-</sup> mice at 12 days post-cannulation (WT n = 8, *Il27ra*<sup>-/-</sup> n = 18) and 19 days post-cannulation (WT n = 18, *Il27ra*<sup>-/-</sup> n = 10). **D**, Representative immunofluorescence and quantification of B cell and CD21+ follicular dendritic cell (FDC) aggregates per gland (WT n = 7, *Il27ra*<sup>-/-</sup> n = 10). **E**, Flow cytometry quantification of GL7+ B cells over total B220+ B cells in SGs from WT mice (n = 10) and *Il27ra*<sup>-/-</sup> mice (n = 10) at 19 days post-cannulation. **F**, Gene expression analysis for *Aicda* in SGs (numbers of mice per group as in C). **G**, Antinuclear antigen-specific serum antibody titer at 19 days post-cannulation, determined by enzyme-linked immunosorbent assay (ELISA) (WT n = 17, *Il27ra*<sup>-/-</sup> n = 16). **H**, Antiadenovirus-specific serum titers at 19 days post-cannulation, determined by ELISA (WT n = 17, *Il27ra*<sup>-/-</sup> n = 16). In **B–F**, symbols represent individual SGs, and in **G** and **H**, symbols represent individual mice; bars show the mean  $\pm$  SEM. \* = P < 0.05; \*\* = P < 0.01; \*\*\* = P < 0.001; \*\*\*\* = P < 0.0001, by Mann-Whitney U test. See Figure 1 for other definitions. Color figure can be viewed in the online issue, which is available at <http://onlinelibrary.wiley.com/doi/10.1002/art.41289/abstract>.

were more abundant and larger in *Il27ra*<sup>-/-</sup> mice (Figures 3A and B and Supplementary Figure 4, <http://onlinelibrary.wiley.com/doi/10.1002/art.41289/abstract>). Consistent with these findings, higher transcripts of *Ltb* and lymphoid chemokines *Cxcl13* and *Ccl19* and their receptors *Cxcr5* and *Ccr7*, which are critical in the development of ELS, were observed in *Il27ra*<sup>-/-</sup> mice than in WT mice, both before (12 days post-cannulation) and concomitant with (19 days post-cannulation) the formation of ELS (Figure 3C). Notably, no differences were observed between uninfected SGs from WT mice and those from *Il27ra*<sup>-/-</sup> mice in histology (Supplementary Figure 4) or ELS-related gene expression (Supplementary

Figure 5A, <http://onlinelibrary.wiley.com/doi/10.1002/art.41289/abstract>).

The proportion of ELS displaying CD21+ FDC networks was significantly higher in cannulated *Il27ra*<sup>-/-</sup> mice compared to controls (Figure 3D). An exaggerated ectopic GC response was also confirmed by a higher prevalence of GL7+ GC B cells in the SGs of *Il27ra*<sup>-/-</sup> mice (Figure 3E) and higher expression levels of activation-induced cytidine deaminase (AID; *Aicda*), the enzyme responsible for somatic hypermutation and class-switch recombination (Figure 3F). Previous studies showed that IL-27 drives IgG2a but not IgG1 Ig class-switching in B cells (26). Accordingly,

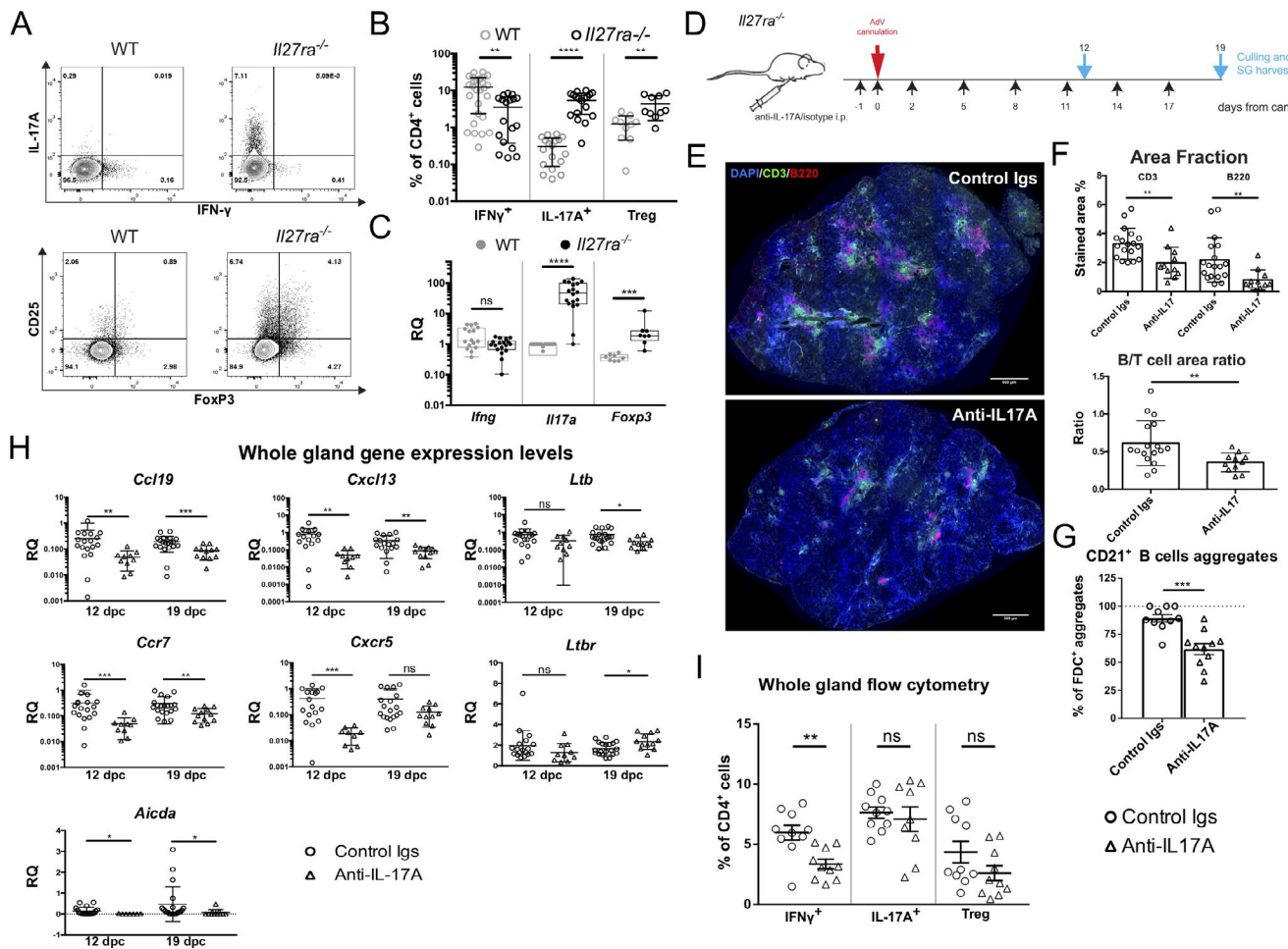


**Figure 4.** Exaggerated ectopic lymphoid structure (ELS) development in *Il27ra*<sup>-/-</sup> mice is mediated by IL-17A. **A**, Representative dot plots of CD4+ T cells from adenovirus-treated wild-type (WT) and *Il27ra*<sup>-/-</sup> mice. **B**, Quantification of interferon- $\gamma$ -positive (IFN $\gamma$ )<sup>+</sup> cells (WT  $n = 41$ , *Il27ra*<sup>-/-</sup>  $n = 18$ ), IL-17 $\alpha$ <sup>+</sup> cells (WT  $n = 32$ , *Il27ra*<sup>-/-</sup>  $n = 18$ ), and FoxP3<sup>+</sup>/CD25<sup>+</sup> cells (WT  $n = 10$ , *Il27ra*<sup>-/-</sup>  $n = 10$ ) as a percentage of CD4<sup>+</sup> T cells in *Il27ra*<sup>-/-</sup> and WT mice. **C**, Real-time quantitative polymerase chain reaction for expression of *Ifng* (WT  $n = 16$ , *Il27ra*<sup>-/-</sup>  $n = 18$ ), *Il17a* (WT  $n = 16$ , *Il27ra*<sup>-/-</sup>  $n = 18$ ), and *Foxp3* (WT  $n = 8$ , *Il27ra*<sup>-/-</sup>  $n = 8$ ) in SG tissue from adenovirus-infected WT and *Il27ra*<sup>-/-</sup> mice. Data are shown as box plots. Each box represents the 25th to 75th percentiles. Lines inside the boxes represent the median. Lines outside the boxes represent the minimum and maximum values. Symbols represent individual mice. **D**, Dosing regimen for IL-17A depletion in vivo. **E**, Representative immunofluorescence for T cells and B cells. **F**, Area fraction of B cell and T cell infiltrates and their ratio in the glands of *Il27ra*<sup>-/-</sup> anti-IL-17A-treated mice ( $n = 11$ ) and Ig-treated mice ( $n = 18$ ). **G**, Quantification of CD21<sup>+</sup> B cell aggregates per gland (Ig  $n = 11$ , anti-IL-17A  $n = 10$ ). **H**, Gene expression in SGs from anti-IL-17A-treated mice and Ig-treated mice at 12 days post-cannulation (Ig  $n = 18$ , anti-IL-17A  $n = 7$ ) and 19 days post-cannulation (Ig  $n = 20$ , anti-IL-17A  $n = 11$ ). **I**, IFN $\gamma$ <sup>+</sup> cells (Ig  $n = 10$ , anti-IL-17A  $n = 10$ ), IL-17 $\alpha$ <sup>+</sup> cells (Ig  $n = 10$ , anti-IL-17A  $n = 9$ ), and FoxP3<sup>+</sup>/CD25<sup>+</sup> cells (Ig  $n = 10$ , anti-IL-17A  $n = 10$ ) as a percentage of CD4<sup>+</sup> T cells in anti-IL-17A-treated and Ig-treated *Il27ra*<sup>-/-</sup> animals at 12 days post-cannulation. In **B**, **F**, **G**, **H**, and **I**, symbols represent individual SGs; bars show the mean  $\pm$  SEM. \* =  $P < 0.05$ ; \*\* =  $P < 0.01$ ; \*\*\* =  $P < 0.001$ ; \*\*\*\* =  $P < 0.0001$ , by Mann-Whitney U test. FDC = follicular dendritic cell (see Figure 1 for other definitions). Color figure can be viewed in the online issue, which is available at <http://onlinelibrary.wiley.com/doi/10.1002/art.41289/abstract>.

we detected higher levels of IgG1 but not IgG2a ANAs and anti-adenovirus antibodies in the sera of *Il27ra*<sup>-/-</sup> mice compared to WT mice (Figures 3G and H). Overall, in our model, IL-27 regulates the magnitude of the local ectopic GC response, and ELS develop unopposed in the absence of a regulatory IL-27 response.

**Uncontrolled expansion of IL-17-producing CD4+ cells drives aberrant ectopic GCs in the SGs of *Il27ra*<sup>-/-</sup> mice, which are restored upon IL-17A blockade.** Given the importance of IL-27 in shaping T cell responses, we speculated that the exaggerated formation and hyperactivity of ELS observed in *Il27ra*<sup>-/-</sup> mice may be due to an early, dysregulated, and imbalanced CD4+ T cell activation in the SGs.

Intracellular flow cytometry on digested SGs at the peak of T cell infiltration (12 days post-cannulation) (Figure 4A) confirmed a striking enrichment in the percentage of IL-17A-producing CD4+ T cells in *Il27ra*<sup>-/-</sup> mice compared to WT mice (Figures 4A and B). This was accompanied by a significant decrease in the percentage of IFN $\gamma$ -producing CD4+ cells (Figures 4A and B). Gene expression analysis showed parallel modulation of *Il17a* and *Il17b* mRNA in the infected SGs (Figure 4C). Consistent with the findings of previous studies that highlighted a role for IL-27 in suppressing inducible Treg cells (28,31), we observed an increased number of FoxP3+/CD25+ Treg cells and elevated gene expression of the transcription factor FoxP3 in cannulated SGs from *Il27ra*<sup>-/-</sup> mice compared to WT mice (Figures 4A–C). The heightened expression of genes involved in both Treg cell differentiation and chemotaxis in the SGs of *Il27ra*<sup>-/-</sup> mice versus WT mice (Supplementary Figure 5B, <http://onlinelibrary.wiley.com/doi/10.1002/art.41289/abstract>) suggests that both phenomena contribute to the increased number of infiltrating FoxP3+/CD25+ Treg cells observed.

To test whether a functional link might exist between the local production of IL-17A and the expansion of ELS in the SGs of *Il27ra*<sup>-/-</sup> mice, we administered a neutralizing anti-IL-17A antibody to *Il27ra*<sup>-/-</sup> mice (Figure 4D). In IL-17A-neutralized mice, we observed smaller and less organized inflammatory foci in the SGs (Figure 4E). A significant reduction in the T cell and B cell compartments was observed following treatment with the anti-IL-17A antibody (Figures 4E and F), restoring the B cell:T cell ratio close to levels observed in WT animals (Figures 3B and 4F), indicating that IL-27 control of ELS composition is mediated through suppression of the Th17/IL-17 response. These changes in ELS following IL-17 neutralization were paralleled by a reduction in the expression of genes required for ELS formation (Figure 4H). Anti-IL-17A-treated animals also displayed a notable reduction in GC function, as shown by a reduction in FDC networks and *Aicda* expression (Figures 4G and H).

Interestingly, we noticed a decrease in the percentage of IFN $\gamma$ - and IL-22-producing cells (Supplementary Figures 6A and B, <http://onlinelibrary.wiley.com/doi/10.1002/art.41289/abstract>) in CD4+ T cell subsets present in the SGs of IL-17A-depleted, adenovirus-infected *Il27ra*<sup>-/-</sup> mice, while Treg cell and IL-17A-producing T cell percentages were unchanged (Figure 4I). Anti-IL-17A treat-

ment did not affect the virus-specific serum IgG1:IgG2a ratio (Supplementary Figure 6C). Taken together, these observations suggest that in our model of viral-induced ELS formation, IL-27 limits the magnitude of SG-infiltrating Th17 cells, and that in the absence of IL-27, IL-17A is responsible for the expansion of ELS and ectopic GC hyperactivation.

**Characterization of CD4+ T cells by dysfunctional IL-17 and IFN $\gamma$  responses to IL-27 in SS.** To reconcile our data showing IL-27-driven inhibition of ELS formation with the apparently contradictory elevation of IL-27 in the SGs of ELS+ SS patients, we investigated whether CD4+ T cells from SS patients displayed an aberrant response to IL-27. We first confirmed that there was no difference between SS patients and healthy donors in surface IL-27R $\alpha$  expression on CD4+ T cells, CD8+ T cells, or B cells (Figure 5A). Although surface expression of IL-27R $\alpha$  was slightly higher in Th17 cells compared to Th1 cells, we did not see major differences in IL-27R $\alpha$  expression on T helper cell subsets between SS patients and healthy donors (Supplementary Figure 1E, <http://onlinelibrary.wiley.com/doi/10.1002/art.41289/abstract>). Similarly, we did not observe any significant difference in the levels of STAT1/3 phosphorylation in the total leukocyte population nor in individual subsets when we stimulated fresh PBMCs with IL-27s in samples from SS patients and healthy donors (Figures 5B and C). We also observed that in our cohort, serum levels of IL-17 were significantly higher in SS patients compared to patients with sicca, and ELS+ patients displayed higher amounts of the cytokine when compared to ELS- patients (Supplementary Figure 1D). This observation suggests that the ability of IL-27 to modulate IL-17 levels may be impaired in SS patients.

To test this hypothesis, cultures of PBMCs from SS patients, RA patients, and age-matched healthy donors were treated with increasing doses of recombinant human IL-27 (0, 40, 100, and 200 ng/ml). Notably, while IL-27 was able to show dose-dependent inhibition of IL-17A-producing CD4+ T cells and IL-17A levels measured in culture supernatants prepared from healthy donor PBMCs, this inhibitory effect was completely lost in SS cultures (Figures 5D–F). Conversely, in PBMC cultures from SS patients, IL-27 favored a significant increase in the secretion of IFN $\gamma$  into culture media and in the frequency of IFN $\gamma$ -producing CD4+ T cells, an effect that was not observed in healthy donor cells (Figures 5D–F). RA patients displayed an intermediate phenotype with a significant reduction in the number of IL-17A-producing CD4+ T cells and a trend toward increased IFN $\gamma$  release (Figures 5D–E), but without a significant reduction in IL-17 release in the supernatant (Figure 5F).

Finally, although previous studies have described IL-27 as a driver of IL-21 production in T helper cells (41,42), IL-27 stimulation of CD4+ T cells from SS patients and healthy donors had no effect on IL-21 secretion, nor on the release of the Th17-associated cytokine IL-22, while a modest increase in IL-10 was seen with the highest dose of IL-27 (Figure 5G). Taken together,

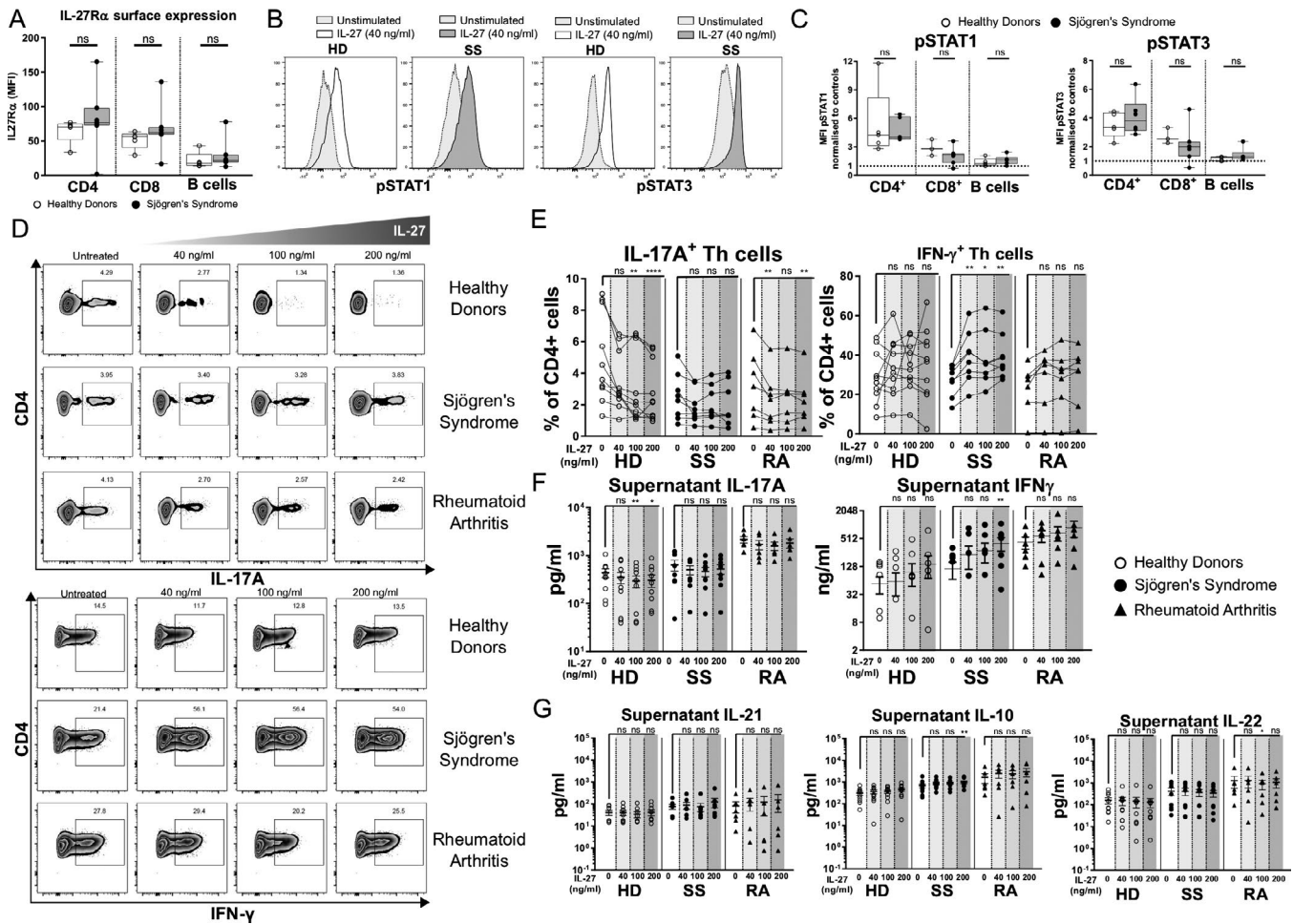


**Figure 5.** CD4+ T cells from Sjögren's syndrome (SS) patients display dysfunctional interleukin-17 (IL-17) and interferon- $\gamma$  (IFN $\gamma$ ) responses to IL-27. **A**, Median fluorescence intensity (MFI) quantification for IL-27 receptor  $\alpha$  (IL-27Ra) on peripheral blood mononuclear cells from SS patients ( $n = 7$ ) and healthy donors (HDs) ( $n = 5$ ). **B**, Representative flow cytometry histograms showing fluorescence intensities for pSTAT1 and pSTAT3 in unstimulated and IL-27-stimulated cells from SS patients and healthy donors. **C**, MFI for pSTAT1 and pSTAT3 in IL-27-stimulated CD4+ cells, CD8+ cells, and CD20+ cells from SS patients ( $n = 6$ ) and healthy donors ( $n = 5$ ). The pSTAT MFI was normalized to that of unstimulated cells. **D**, Representative dot plots for IL-17A- and IFN $\gamma$ -producing CD4+ T cells in peripheral blood mononuclear cells from SS patients, rheumatoid arthritis (RA) patients, and healthy donors, cultured for 3 days with indicated doses of recombinant IL-27. Numbers indicate gated population as a percentage of total CD4+ T cells. **E**, Cytokine-producing CD4+ T cells (SS  $n = 8$ , RA  $n = 7$ , healthy donors  $n = 10$ ). **F** and **G**, Levels of IL-17A, IFN $\gamma$ , IL-21, IL-10, and IL-22 in cell culture supernatant (SS  $n = 8$ , RA  $n = 6$ , healthy donors  $n = 10$ ). In **A** and **C**, data are shown as box plots. Each box represents the 25th to 75th percentiles. Lines inside the boxes represent the median. Lines outside the boxes represent the minimum and maximum values. Symbols represent individual subjects.  $P$  values (all not significant [NS]) were determined by Mann-Whitney U test. In **E-G**, symbols represent individual samples; bars show the mean  $\pm$  SEM. \* =  $P < 0.05$ , \*\* =  $P < 0.01$ , \*\*\*\* =  $P < 0.0001$ , by Friedman's test with Dunn's correction for multiple comparisons.

these data demonstrate that upon IL-27 stimulation, CD4+ T cells from SS patients display a marked resistance to down-regulation of IL-17A production and an aberrant IFN $\gamma$  response. This behavior is restricted to SS patients.

**DISCUSSION**

We have recently shown that, in the context of ELS, when functional IL-27 signaling is missing, lymphoid aggregates with some resemblance to ELS developed in the synovium of a model of experimental arthritis normally devoid of ELS (40). However, in

this model, the impact on the local humoral autoimmune response, together with the underlying mechanisms governing ELS formation, remained elusive. Here, in the present inducible model of ELS formation, we have shown that the absence of a functional IL-27 signaling results in the heightened expression of key genes involved in ELS formation, the development of larger ELS with enriched B cell infiltration, and the presence of accelerated and enhanced ectopic GC responses.

Consistent with the reported inhibitory role of IL-27 in Th17 differentiation (27,29), we observed a remarkable expansion of IL-17-producing CD4+ T cells in the SGs of *Il27ra*<sup>-/-</sup> mice, which

was accompanied by a reduction in the local Th1 response. Furthermore, an increase in SG-infiltrating FoxP3+ CD4+ T cells was also observed in the absence of IL-27 signaling, which is in keeping with the ability of this cytokine to inhibit inducible Treg cell differentiation (28). We speculated that the dysregulated formation of ELS in *Il27ra*<sup>-/-</sup> mice was due to a loss of an inhibitory IL-27 signal on Th17 differentiation. Treatment of *Il27ra*<sup>-/-</sup> mice with an anti-IL-17A antibody during adenovirus infection almost completely reversed the excessive GC responses seen in the SGs and restored the cellular composition of the ELS, with a significant reduction in B cell involvement and CD21+ FDC networks, thereby confirming our hypothesis. Notably, preventive IL-17A blockade did not completely inhibit the development of ELS in *Il27ra*<sup>-/-</sup> mice, suggesting a role for the IL-27/Th17 effector response in controlling the propagation rather than the formation of ELS in our model.

While the role of IL-17A in autoimmunity is well established, the relationship between IL-27, clinical disease progression, and Th17-mediated diseases in humans remains ill-defined. In the present study, we not only observed higher local and systemic levels of IL-27 in SS patients compared to patients with sicca symptoms, but for the first time we showed that in SS SGs, the IL-27p28 protein signal prevalently colocalized with DC-LAMP+ mature dendritic cells (but not CD68+ macrophages), which were heavily enriched within the T cell-rich areas of the lymphoid aggregates. Similarly, high expression of *Il27* mRNA was observed in CD11b+ myeloid cells isolated from murine SG, synchronous to the infiltration of CD4+ T cells in our model. These data suggest that activated dendritic cells are a key source of IL-27 in both mouse and human pathology and primarily exert their function by shaping the CD4+ T cell response. In our murine model, at later stages of ELS formation, T cells became the prominent producers of IL-27p28. While this is consistent with other recent observations in mice (43), we could not confirm IL-27 production in T cells from the SGs of ELS+ SS patients. This suggests that IL-27-producing T cells may be important for the resolution phase of ELS but are absent in the persistent inflammation observed in patients with SS.

Unexpectedly, and opposite to what we previously reported in the RA synovium (40), local IL-27 expression was found to be selectively increased in ELS+ SS patients compared to ELS-patients. Notably, CD4+ T cells from patients with SS were resistant to the immunoregulatory effects of IL-27. Upon incubation with IL-27, we observed a dose-dependent down-regulation of IL-17 production in CD4+ T cells from healthy individuals, while SS patients consistently failed to down-modulate IL-17 production and instead displayed exaggerated IFN $\gamma$  secretion. These effects were not due to differences in the presence or expression levels of the IL-27R in CD4+ T cells from SS patients, or due to obvious defects in the activation of signaling pathways immediately downstream of IL-27. Thus, in SS patients,

despite an increased expression of IL-27 during active disease, impaired IL-27 responsiveness leading to an aberrant control of IL-17 and an excessive IFN $\gamma$  response may contribute to the higher degree of SG immunopathology and ELS development observed. Consistent with this hypothesis, Th17 overactivation has been associated with the early phases of SG inflammation and the formation of ectopic GCs (44), while hyperactivation of type II IFN has been advocated as a biomarker of lymphoma development in SS (45).

While our model displays several clinical features of human SS, the lack of sustained chronicity does not allow for an evaluation of the long-term consequences of the aberrant ectopic GC response. When we extended our observations to patients with SS, we unraveled the existence of profoundly altered responsiveness to IL-27 in CD4+ T cells. These studies were limited to in vitro approaches that need to be extended in order to pinpoint underlying mechanisms responsible for the defective IL-27 immunoregulatory checkpoint observed. Overall, our findings establish IL-27 as a key suppressor of ectopic GC development and suggest that reestablishing the functional immunomodulation of the IL-27/Th17 axis could have therapeutic potential in controlling ELS+ autoantibody-mediated diseases such as SS.

## ACKNOWLEDGMENT

We thank the BCI/WHRI Flow Cytometry Core Facility staff for their technical assistance.

## AUTHOR CONTRIBUTIONS

All authors were involved in drafting the article or revising it critically for important intellectual content, and all authors approved the final version to be published. Dr. Lucchesi had full access to all of the data in the study and takes responsibility for the integrity of the data and the accuracy of the data analysis.

**Study conception and design.** Lucchesi, Coleby, Pontarini, S. Jones, Humphreys, Sutcliffe, Tappuni, Pitzalis, G. Jones, Bombardieri.

**Acquisition of data.** Lucchesi, Coleby, Pontarini, Prediletto, Rivellesse, Hill, Soria, G. Jones.

**Analysis and interpretation of data.** Lucchesi, Coleby, Pontarini, G. Jones, Bombardieri.

## REFERENCES

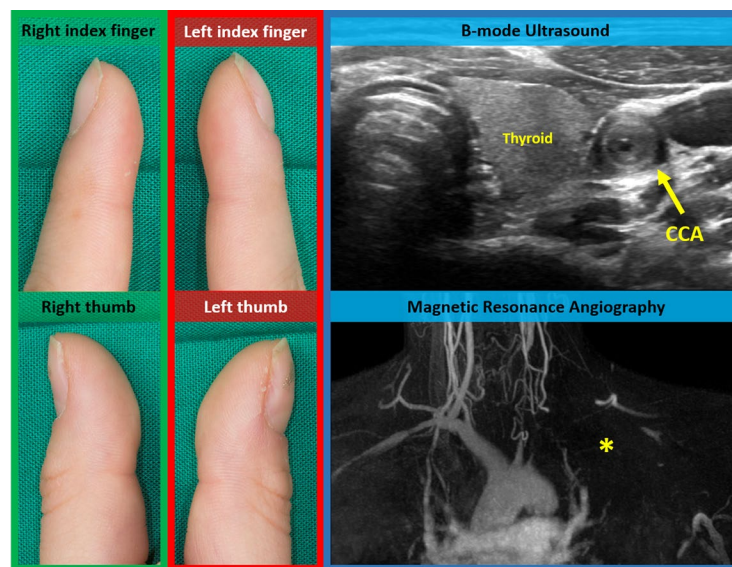
1. Pitzalis C, Jones GW, Bombardieri M, Jones SA. Ectopic lymphoid-like structures in infection, cancer and autoimmunity [review]. *Nat Rev Immunol* 2014;14:447–62.
2. Jones GW, Jones SA. Ectopic lymphoid follicles: inducible centres for generating antigen-specific immune responses within tissues. *Immunology* 2015;147:141–51.
3. Bombardieri M, Lewis M, Pitzalis C. Ectopic lymphoid neogenesis in rheumatic autoimmune diseases [review]. *Nat Rev Rheumatol* 2017;13:141–54.
4. Mavragani CP, Moutsopoulos HM. Sjögren's syndrome [review]. *Annu Rev Pathol Mech Dis* 2013;9:130919210859006.
5. Ramos-Casals M, Brito-Zerón P, Sisó-Almirall A, Bosch X. Primary Sjögren syndrome. *BMJ* 2012;344:e3821.

6. Barone F, Bombardieri M, Manzo A, Blades MC, Morgan PR, Challacombe SJ, et al. Association of CXCL13 and CCL21 expression with the progressive organization of lymphoid-like structures in Sjögren's syndrome. *Arthritis Rheum* 2005;52:1773–84.
7. Jonsson MV, Skarstein K, Jonsson R, Brun JG. Serological implications of germinal center-like structures in primary Sjögren's syndrome. *J Rheumatol* 2007;34:2044–9.
8. Theander E, Vasaitis L, Baecklund E, Nordmark G, Warfvinge G, Liedholm R, et al. Lymphoid organisation in labial salivary gland biopsies is a possible predictor for the development of malignant lymphoma in primary Sjögren's syndrome. *Ann Rheum Dis* 2011;70:1363–8.
9. Bombardieri M, Barone F, Humby F, Kelly S, McGurk M, Morgan P, et al. Activation-induced cytidine deaminase expression in follicular dendritic cell networks and interfollicular large B cells supports functionality of ectopic lymphoid neogenesis in autoimmune sialoadenitis and MALT lymphoma in Sjögren's syndrome. *J Immunol* 2007;179:4929–38.
10. Haacke EA, van der Vegt B, Vissink A, Spijkervet FK, Bootsma H, Kroese FG. Germinal centres in diagnostic labial gland biopsies of patients with primary Sjögren's syndrome are not predictive for parotid MALT lymphoma development. *Ann Rheum Dis* 2017;76:1781–4.
11. Sène D, Ismaël S, Forien M, Charlotte F, Kaci R, Cacoub P, et al. Ectopic germinal center-like structures in minor salivary gland biopsy tissue predict lymphoma occurrence in patients with primary Sjögren's syndrome. *Arthritis Rheumatol* 2018;70:1481–8.
12. Risselada AP, Kruize AA, Goldschmeding R, Lafeber FP, Bijlsma JW, van Roon JA. The prognostic value of routinely performed minor salivary gland assessments in primary Sjögren's syndrome. *Ann Rheum Dis* 2014;73:1537–40.
13. Jones GW, Hill DG, Cardus A, Jones SA. IL-27: a double agent in the IL-6 family. *Clin Exp Immunol* 2018;193:37–46.
14. Yoshida H, Hunter CA. The immunobiology of interleukin-27 [review]. *Annu Rev Immunol* 2015;33:417–443.
15. Liu FD, Kenngott EE, Schröter MF, Kühl A, Jennrich S, Watzlawick R, et al. Timed action of IL-27 protects from immunopathology while preserving defense in influenza. *PLoS Pathog* 2014;10:e1004110.
16. Artis D, Villarino A, Silverman M, He W. The IL-27 receptor (WSX-1) is an inhibitor of innate and adaptive elements of type 2 immunity. *Am Assoc Immunol* 2004;173:5626–34.
17. Clement M, Marsden M, Stacey MA, Abdul-Karim J, Gimeno Brias S, Costa Bento D, et al. Cytomegalovirus-specific IL-10-producing CD4+ T cells are governed by type-I IFN-induced IL-27 and promote virus persistence. *PLoS Pathog* 2016;12:e1006050.
18. Takeda A, Hamano S, Yamanaka A, Hanada T, Ishibashi T, Mak TW, et al. Cutting edge: role of IL-27/WSX-1 signaling for induction of T-bet through activation of STAT1 during initial Th1 commitment. *J Immunol* 2003;170:4886–90.
19. Morishima N, Mizoguchi I, Okumura M, Chiba Y, Xu M, Shimizu M, et al. A pivotal role for interleukin-27 in CD8+ T cell functions and generation of cytotoxic T lymphocytes. *J Biomed Biotechnol* 2010;2010:1–10.
20. Villarino A, Hibbert L, Wilson E, Yoshida H, Kastelein RA, Hunter CA. The IL-27R (WSX-1) is required to suppress T cell hyperactivity during infection. *Immunity* 2003;19:645–55.
21. Villarino AV, Stumhofer JS, Saris CJ, Kastelein RA, de Sauvage FJ, Hunter CA. IL-27 limits IL-2 production during Th1 differentiation. *J Immunol* 2006;176:237–47.
22. Owaki T, Asakawa M, Kamiya S, Takeda K. IL-27 suppresses CD28-mediated IL-2 production through suppressor of cytokine signaling 3. *Am Assoc Immunol* 2006;176:2773–80.
23. Stumhofer JS, Silver JS, Laurence A, Porrett PM, Harris TH, Turka LA, et al. Interleukins 27 and 6 induce STAT3-mediated T cell production of interleukin 10. *Nat Immunol* 2007;8:1363–71.
24. Shen W, Hixon JA, McLean MH, Li WQ, Durum SK. IL-22-expressing murine lymphocytes display plasticity and pathogenicity in reporter mice. *Front Immunol* 2016;6:1814.
25. Hunter CA, Kastelein R. Interleukin-27: balancing protective and pathological immunity. *Immunity* 2012;37:960–9.
26. Yoshimoto T, Okada K, Morishima N. Induction of IgG2a class switching in B cells by IL-27. *Am Assoc Immunol* 2004;173:2479–85.
27. Diveu C, McGeachy MJ, Boniface K, Stumhofer JS, Sathe M, Joyce-Shaikh B, et al. IL-27 blocks RORc expression to inhibit lineage commitment of Th17 cells. *J Immunol* 2009;182:5748–56.
28. Neufert C, Becker C, Wirtz S, Fantini MC, Weigmann B, Galle PR, et al. IL-27 controls the development of inducible regulatory T cells and Th17 cells via differential effects on STAT1. *Eur J Immunol* 2007;37:1809–16.
29. Stumhofer JS, Laurence A, Wilson EH, Huang E, Tato CM, Johnson LM, et al. Interleukin 27 negatively regulates the development of interleukin 17-producing T helper cells during chronic inflammation of the central nervous system. *Nat Immunol* 2006;7:937–45.
30. Hall AO, Beiting DP, Tato C, John B, Oldenhove G, Lombana CG, et al. The cytokines interleukin 27 and interferon- $\gamma$  promote distinct Treg cell populations required to limit infection-induced pathology. *Immunity* 2012;37:511–23.
31. Huber M, Steinwald V, Guralnik A, Brüstle A, Kleemann P, Rosenplänter C, et al. IL-27 inhibits the development of regulatory T cells via STAT3. *Int Immunol* 2007;20:223–34.
32. Bombardieri M, Barone F, Lucchesi D, Nayar S, van den Berg WB, Proctor G, et al. Inducible tertiary lymphoid structures, autoimmunity, and exocrine dysfunction in a novel model of salivary gland inflammation in C57BL/6 mice. *J Immunol* 2012;189:3767–76.
33. Croia C, Astorri E, Murray-Brown W, Willis A, Brokstad KA, Sutcliffe N, et al. Implication of Epstein-Barr virus infection in disease-specific autoreactive B cell activation in ectopic lymphoid structures of Sjögren's syndrome. *Arthritis Rheumatol* 2014;66:2545–57.
34. Yoshida H, Hamano S, Senaldi G, Covey T, Faggioni R, Mu S, et al. WSX-1 is required for the initiation of Th1 responses and resistance to L. major infection. *Immunity* 2001;15:569–78.
35. Schindelin J, Arganda-Carreras I, Frise E, Kaynig V, Longair M, Pietzsch T, et al. Fiji: an open-source platform for biological-image analysis. *Nat Methods* 2012;9:676–82.
36. Bankhead P, Loughrey MB, Fernández JA, Dombrowski Y, McArt DG, Dunne PD, et al. QuPath: open source software for digital pathology image analysis. *Sci Rep* 2017;7:16878.
37. Pontarini E, Lucchesi D, Fossati-Jimack L, Coleby R, Tentorio P, Croia C, et al. NK cell recruitment in salivary glands provides early viral control but is dispensable for tertiary lymphoid structure formation. *J Leukoc Biol* 2019;105:589–602.
38. Barone F, Nayar S, Campos J, Cloake T, Withers DR, Toellner KM, et al. IL-22 regulates lymphoid chemokine production and assembly of tertiary lymphoid organs. *Proc Natl Acad Sci U S A* 2015;112:11024–9.
39. Pflanz S, Timans JC, Cheung J, Rosales R, Kanzler H, Gilbert J, et al. IL-27, a heterodimeric cytokine composed of EBI3 and p28 protein, induces proliferation of naive CD4+ T cells. *Immunity* 2002;16:779–90.
40. Jones GW, Bombardieri M, Greenhill CJ, McLeod L, Nerviani A, Rocher-Ros V, et al. Interleukin-27 inhibits ectopic lymphoid-like structure development in early inflammatory arthritis. *J Exp Med* 2015;212:793–802.
41. Batten M, Ramamoorthi N, Kljavin NM, Ma CS, Cox JH, Dengler HS, et al. IL-27 supports germinal center function by enhancing IL-21 production and the function of T follicular helper cells. *J Exp Med* 2010;207:2895–906.

42. Pot C, Jin H, Awasthi A, Liu SM, Lai CY, Madan R, et al. Cutting edge: IL-27 induces the transcription factor c-Maf, cytokine IL-21, and the costimulatory receptor ICOS that coordinately act together to promote differentiation of IL-10-producing Tr1 cells. *J Immunol* 2009;183:797–801.
43. Kimura D, Miyakoda M, Kimura K, Honma K, Hara H, Yoshida H, et al. Interleukin-27-producing CD4+ T cells regulate protective immunity during malaria parasite infection. *Immunity* 2016;44:672–82.
44. Verstappen GM, Corneth OB, Bootsma H, Kroese FG. Th17 cells in primary Sjögren's syndrome: pathogenicity and plasticity. *J Autoimmun* 2018;87:16–25.
45. Nezos A, Gravani F, Tassidou A, Kapsogeorgou EK, Voulgarelis M, Koutsilieris M, et al. Type I and II interferon signatures in Sjögren's syndrome pathogenesis: contributions in distinct clinical phenotypes and Sjögren's related lymphomagenesis. *J Autoimmun* 2015;63:47–58.

DOI 10.1002/art.41313

### Clinical Images: Unilateral Hippocratic fingers and macaroni sign



The patient, a 17-year-old girl, presented to the emergency department with a 2-week history of pain in her left arm and swelling of the fingers on her left hand. Her history was otherwise unremarkable. Notably, there were no symptoms of systemic inflammation (night sweats, fever, or weight loss). Clinical examination of the left arm revealed absence of pulses. Blood pressure was low (systolic 50 mm Hg) when measured on the left arm and elevated (170/100 mm Hg) when measured on the right arm. Physical examination revealed finger clubbing (Hippocratic fingers) only on the left hand. The C-reactive protein level was mildly elevated (1.8 mg/dl [normal <0.5]). Color duplex sonography showed filiform long-segment stenosis in the left common carotid artery (CCA) with marked concentric intimal thickening (arrow). This sonographic feature, known as macaroni sign, confirmed the diagnosis of Takayasu arteritis (TAK). Ultrasound and magnetic resonance angiography revealed an occlusion of the left subclavian and axillary artery (asterisk) as an underlying cause of finger clubbing on the left hand. Further imaging also revealed significant bilateral renal artery stenosis causing renovascular hypertension. Immunosuppressive and antihypertensive treatment was initiated. Subsequently, renal artery stenosis was treated with stent angioplasty. Bilateral clubbing can be seen in patients with severe cardiopulmonary disease, classically in patients with congenital cyanotic heart disease. Unilateral clubbing is a very rare presentation of TAK, resulting from severe chronic upper limb ischemia (1–3).

1. Kaditis AG, Nelson AM, Driscoll DJ. Takayasu's arteritis presenting with unilateral digital clubbing. *J Rheumatol* 1995;22:2346–8.
2. Ishikawa M, Okada J, Kondo H. Takayasu's arteritis with transient clubbed finger. *Clin Exp Rheumatol* 1999;17:629–30.
3. Çivilibal M, Selçuk Duru N, Doğdu G, Elevli M, Ayta S. A Takayasu's arteritis case with unilateral digital clubbing. *Turk J Rheumatol* 2011;26:163–6.

Christian Lottspeich, MD   
 Michael Czihal, MD  
 Medical Clinic and Policlinic IV  
 Hospital of the Ludwig-Maximilians-University  
 Annette Friederike Jansson, MD  
 Ava Oberlack, MD  
 Dr. von Hauner Children's Hospital  
 Hospital of the Ludwig-Maximilians-University  
 Munich, Germany